

# Samplets: Wavelet concepts for scattered data

Helmut Harbrecht and Michael Multerer

**Abstract** This chapter is dedicated to recent developments in the field of wavelet analysis for scattered data. We introduce the concept of samplets, which are signed measures of wavelet type and may be defined on sets of arbitrarily distributed data sites in possibly high dimension. By employing samplets, we transfer well-known concepts known from wavelet analysis, namely the fast basis transform, data compression, operator compression and operator arithmetics to scattered data problems. Especially, samplet matrix compression facilitates the rapid solution of scattered data interpolation problems, even for kernel functions with nonlocal support. Finally, we demonstrate that sparsity constraints for scattered data approximation problems become meaningful and can efficiently be solved in samplet coordinates.

## 1 Introduction

Multiresolution methods and especially wavelet techniques have a long standing tradition and are a versatile tool in various fields. Applications comprise, among others, nonlinear approximation, image analysis, signal processing and machine learning, see for instance [16, 20, 25, 27, 55, 56] and the references therein. Starting from a signal, the pivotal idea of wavelet techniques is the splitting of this signal into its contributions relative to a hierarchy of scales. Such a *multiresolution analysis* starts from an approximation on a coarse scale and successively resolves details, that have not been captured so far, at finer scales. Wavelet techniques naturally accommodate data compression and adaptivity. The great success of wavelet techniques has

---

Helmut Harbrecht

Departement Mathematik und Informatik, Universität Basel, Spiegelgasse 1, 4051 Basel, Schweiz,  
e-mail: helmut.harbrecht@unibas.ch

Michael Multerer

Istituto Eulerio, Università della Svizzera italiana, Via la Santa 1, 6962 Lugano, Svizzera, e-mail:  
michael.multerer@usi.ch

specifically been triggered by the fast wavelet transform, which transforms a signal into its wavelet representation and back, that can be computed with linear cost in terms of the size of the wavelet basis, see [18, 54].

The original construction of wavelets is based on dilations and translations of a given mother wavelet. This way, a nested sequence of approximation spaces is obtained and the elements of this sequence are scaled copies of each other. This construction of wavelets is limited to structured data, such as uniform subdivisions of the real line. Adaptions to deal with bounded intervals have been suggested in e.g. [2, 17, 22], while wavelet constructions on manifolds are the topic of e.g. [24, 44, 75]. An extension to surface triangulations, has been suggested in [71], where (multi-)wavelets are constructed as linear combinations of functions at a fixed fine scale. The stability of the resulting *Tausch-White wavelet basis* follows from its orthonormality. Another approach to construct a multiresolution analysis on unstructured data, for example on graphs, are *diffusion wavelets*, see [19]. However, there is no linear cost bound for the computation of a diffusion wavelet basis.

This chapter is a survey on the generalization of the Tausch-White wavelet construction towards general scattered data. This is achieved by abstracting the construction [1, 71] towards discrete signed measures. The result is multiresolution analysis of discrete signed measures of localized support that we call *samplets*. Samplets are tailored to the underlying data sites and may be computed such that they exhibit *vanishing moments*, that is their associated measure integrals. Lowest order samplets, which resemble Haar wavelets on scattered data have been considered in the past for data compression in [62]. It is worth mentioning that the construction of samplets is not limited to the use of polynomial vanishing moments. Indeed, it is easily possible to adapt the presented concepts to primitives with different desired properties.

We present a general construction template for samplets with an arbitrary number of vanishing moments. This construction can always be performed with linear cost for a balanced cluster tree for the data sites, even for non-quasi-uniform data sites. The resulting basis is always orthonormal and hence stable. Due to the vanishing moments, the coefficients in the representation of scattered data with respect to samplet coordinates decay fast whenever the data values resemble a smooth function evaluated at the data sites. This straightforwardly enables data compression. In contrast, non-smooth regions in the data are indicated by large samplet coefficients. This, in turn, enables feature detection and extraction.

Similar to wavelet matrix compression [6, 21, 23, 67, 74], samplets are applicable for the compression of kernel matrices. Such matrices arise in the scattered data approximation context, compare [30, 46, 66, 76, 77, 78]. Kernel matrices are typically densely populated since the underlying reproducing kernels are nonlocal. Nonetheless, the kernels are typically *asymptotically smooth*, meaning that they behave like smooth functions apart from the diagonal. Hence, the discretization of such kernel matrices by samplets with vanishing moments results in quasi-sparse kernel matrices. They can be compressed such that only a sparse matrix remains. The resulting compression pattern has been derived in [41]. Furthermore, as shown in [43], a respective matrix algebra can be defined.

Samplers provide a meaningful interpretation of *sparsity constraints* for scattered data, since the representation of data itself becomes sparse. Such constraints have a wide applicability in machine learning, statistics, as well as in signal processing. Examples for the latter are deblurring, feature selection and compressive sensing, see [11, 14, 29, 49, 70]. In practice, sparsity constraints are imposed by adding an  $\ell^1$ -regularization term to the objective function. Dealing with this regularization in an efficient way is especially mandatory for *basis pursuit*, that is, for decomposing given data into an optimal superposition of dictionary elements, where optimal means having the smallest  $\ell^1$ -norm of coefficients among all such decompositions, see, for example, [15, 57, 73]. We demonstrate that the basis pursuit problem can efficiently be solved within a the sampler basis and reconstruct scattered data using a dictionary of multiple kernels.

The rest of this chapter is organized as follows. In Section 2, multiresolution analyses for scattered data and the concept of samplers are introduced. The change of basis by means of the fast sampler transform and resulting applications are the topic of Section 3. Section 4 deals with scattered data approximation in reproducing kernel Hilbert spaces. Here, we especially introduce the sampler compression of kernel matrices and the efficient treatment of sparsity constraints by the semi-smooth Newton method.

Throughout this chapter, in order to avoid the repeated use of generic but unspecified constants, by  $C \lesssim D$  we indicate that  $C$  can be bounded by a multiple of  $D$ , independently of parameters which  $C$  and  $D$  may depend on. Moreover,  $C \gtrsim D$  is defined as  $D \lesssim C$  and  $C \sim D$  as  $C \lesssim D$  and  $D \lesssim C$ .

## 2 Multiresolution analysis of scattered data

### 2.1 Sampler bases

Let  $X := \{\mathbf{x}_1, \dots, \mathbf{x}_N\} \subset \Omega$  denote a set of *data sites* within some bounded or unbounded region  $\Omega \subset \mathbb{R}^d$ . Associated to these data sites, we introduce the Dirac- $\delta$ -distributions

$$\delta_{\mathbf{x}_1}, \dots, \delta_{\mathbf{x}_N} \in [C(\Omega)]', \quad (1)$$

where we endow  $C(\Omega)$  with the sup-norm. The Dirac- $\delta$ -distributions satisfy

$$(f, \delta_{\mathbf{x}_i})_\Omega := \delta_{\mathbf{x}_i}(f) = f(\mathbf{x}_i) \text{ for all } f \in C(\Omega)$$

and serve as *information functionals* of some, maybe unknown, function  $f \in C(\Omega)$ . In this setting, the *data values*  $f_i := (f, \delta_{\mathbf{x}_i})_\Omega$ ,  $i = 1, \dots, N$ , amount to the available information of the function  $f$ , compare [59].

By the Riesz representation theorem, the dual space  $[C(\Omega)]'$  is isometrically isomorphic to the space of regular, finitely additive signed measures of bounded variation on  $\Omega$ , equipped with the total variation norm. We call this space by  $\text{rba}(\Omega)$ , as

usual. For each  $\ell \in [C(\Omega)]'$ , there exists a signed measure  $\mu_\ell \in \text{rba}(\Omega)$  such that

$$\ell_\mu(f) = \int_{\Omega} f(\mathbf{x}) d\mu(\mathbf{x}) \text{ for all } f \in C(\Omega),$$

and vice versa, see [61]. In view of this identification, we interchangeably consider the Dirac  $\delta$ -distributions from (1) as linear functionals or as measures.

The Dirac- $\delta$ -distributions span the linear subspace

$$\mathcal{X} := \text{span}\{\delta_{\mathbf{x}_1}, \dots, \delta_{\mathbf{x}_N}\} \subset [C(\Omega)]'$$

containing all discrete and finite signed measures supported at the data sites in  $X$ . Endowed with the bilinear form  $\langle \cdot, \cdot \rangle_{\mathcal{X}} : \mathcal{X} \times \mathcal{X} \rightarrow \mathbb{R}$  with  $\langle \delta_{\mathbf{x}_i}, \delta_{\mathbf{x}_j} \rangle_{\mathcal{X}} = m_{i,j}$ , where  $\mathbf{M} = [m_{i,j}]_{i,j=1}^N \in \mathbb{R}^{N \times N}$  is a symmetric and positive definite matrix, the space  $\mathcal{X}$  becomes a Hilbert space. For arbitrary  $u', v' \in \mathcal{X}$ , the inner product is given by

$$\langle u', v' \rangle_{\mathcal{X}} = \sum_{i,j=1}^N m_{i,j} u_i v_j, \text{ where } u' = \sum_{i=1}^N u_i \delta_{\mathbf{x}_i}, v' = \sum_{i=1}^N v_i \delta_{\mathbf{x}_i}.$$

The canonical choice for  $\mathbf{M}$  is the identity matrix, which renders the space  $\mathcal{X}$  is isometrically isomorphic to  $\mathbb{R}^N$  with the Euclidean inner product.

Given a *multiresolution analysis*

$$\mathcal{X}_0 \subset \mathcal{X}_1 \subset \dots \subset \mathcal{X}_J = \mathcal{X},$$

we keep track of the increment of information between two consecutive levels  $j$  and  $j+1$ . Since there holds  $\mathcal{X}_j \subset \mathcal{X}_{j+1}$ , we may (orthogonally) decompose

$$\mathcal{X}_{j+1} = \mathcal{X}_j \oplus^{\perp} \mathcal{S}_j$$

for a certain *detail space*  $\mathcal{S}_j$ . In analogy to wavelet nomenclature, we call the elements of a basis of  $\mathcal{X}_0$  *scaling distributions* and the elements of a basis of one of the spaces  $\mathcal{S}_j$  *samplets*. This name is motivated by the idea that the basis distributions in  $\mathcal{S}_j$  are supported at a small subsample or samplet of the data sites in  $X$ . The collection of the bases of  $\mathcal{S}_j$  for  $j = 0, \dots, J-1$  together with a basis of  $\mathcal{X}_0$  is called a *samplet basis* for  $\mathcal{X}$ .

To enable data compression, we assume that the samplets have *vanishing moments* of order  $q+1$ , viz.,

$$(p, \sigma_{j,k})_{\Omega} = 0 \text{ for all } p \in \mathcal{P}_q, \quad (2)$$

where  $\mathcal{P}_q := \text{span}\{\mathbf{x}^{\alpha} : \|\alpha\|_1 \leq q\}$  denotes the space of all polynomials with total degree at most  $q$ . In view of larger spatial dimension  $d$ , we observe that the dimension of  $\mathcal{P}_q$  is



$$m_q := \dim(\mathcal{P}_q) = \binom{q+d}{d} = \frac{(d+q) \cdots (d+1)}{q!} = \mathcal{O}(d^q). \quad (3)$$

Hence, the number of vanishing moment conditions only grows polynomially with respect to  $d$ .

Following the discrete signed measure interpretation of samplers, equation (2) implies that a sampler amounts to a quadrature formula, which annihilates polynomials up to order  $q+1$ .

## 2.2 Cluster tree

To construct an orthonormal sampler basis with vanishing moments, see (2), we adapt the wavelet construction from [71] to the scattered data framework. The first step is to construct a hierarchy of subspaces of signed measures. To this end, we perform a hierarchical clustering of the set  $X$  with respect to the Euclidean distance. This approach amounts to a clustering of the Dirac- $\delta$ -distributions spanning  $\mathcal{X}$  by means of the Wasserstein distance  $W_p(\delta_{\mathbf{x}_i}, \delta_{\mathbf{x}_j}) = \|\mathbf{x}_i - \mathbf{x}_j\|_2$  for any  $p \geq 1$ .

**Definition 1.** Let  $\mathcal{T} = (V, E)$  be a tree with vertices  $V$  and edges  $E$ . For  $\tau \in V$ , we denote the set of *children* of  $\tau$  by  $\text{child}(\tau)$ . The set of *leaves* is defined as  $\mathcal{L}(\mathcal{T}) := \{\tau \in V : \text{child}(\tau) = \emptyset\}$ .

The tree  $\mathcal{T}$  is a *cluster tree* for the set  $X$ , iff  $X$  is the root of  $\mathcal{T}$  and all  $\tau \in V \setminus \mathcal{L}(\mathcal{T})$  are disjoint unions of their children, viz.,  $\tau = \cup_{\tau' \in \text{child}(\tau)} \tau'$ . The *level*  $\text{level}(\tau)$  of  $\tau \in \mathcal{T}$  is its distance from the root. Finally, the *depth*  $J$  of  $\mathcal{T}$  is the maximum level of all clusters.

*Remark 1.* There exist different possibilities to construct a cluster tree for the set  $X$ . We focus on binary trees and remark that other options, such as  $2^d$ -trees, may be considered with the obvious modifications.

Definition 1 provides a hierarchical structure for the set  $X$ . Even so, it does not provide guarantees for the cardinalities of the clusters. To account for this issue, we introduce the concept of a *balanced binary tree*.

**Definition 2.** Let  $\mathcal{T}$  be a cluster tree for  $X$  with depth  $J$ . We call  $\mathcal{T}$  a *balanced binary tree*, iff all clusters  $\tau$  satisfy the following two conditions:

- (i) The cluster  $\tau$  has exactly two children if  $\text{level}(\tau) < J$ . It has no children if  $\text{level}(\tau) = J$ .
- (ii) There holds  $|\tau| \sim 2^{J-\text{level}(\tau)}$ , where  $|\tau|$  denotes the number of points contained in  $\tau$ .

A balanced binary tree can be constructed by *cardinality balanced clustering*. This means that the root cluster  $X$  is split into two child clusters of identical (or similar) cardinality. This process is repeated recursively for the resulting child clusters until their cardinality falls below a given threshold. For the subdivision, the cluster's

bounding box is split along its longest edge such that the resulting two boxes both contain an equal number of points. Thus, as the cluster cardinality halves with each level, we obtain  $\mathcal{O}(\log N)$  levels in total. The cost per level is  $\mathcal{O}(N)$  if the subdivision is performed with respect to the median, compare [8]. The overall cost for constructing the cluster tree is therefore  $\mathcal{O}(N \log N)$ .

We remark that a balanced tree is only required to guarantee the cost bounds for the presented algorithms. The error and compression estimates presented later on are robust in the sense that they are formulated directly in terms of the actual cluster sizes rather than the introduced cluster level.

### 2.3 Construction of the samplers

Given a cluster tree, we start by introducing a *two-scale transform* between basis elements on a cluster  $\tau$  of level  $j$ . To this end, we represent scaling distributions  $\Phi_j^\tau = \{\varphi_{j,k}^\tau\}$  and samplers  $\Sigma_j^\tau = \{\sigma_{j,k}^\tau\}$  recursively as linear combinations of the scaling distributions  $\Phi_{j+1}^\tau$  of  $\tau$ 's child clusters. This amounts to the *refinement relations*

$$\varphi_{j,k}^\tau = \sum_{\ell=1}^{n_{j+1}^\tau} q_{j,\Phi,\ell,k}^\tau \varphi_{j+1,\ell}^\tau \text{ and } \sigma_{j,k}^\tau = \sum_{\ell=1}^{n_{j+1}^\tau} q_{j,\Sigma,\ell,k}^\tau \varphi_{j+1,\ell}^\tau \text{ with } n_{j+1}^\tau := |\Phi_{j+1}^\tau|,$$

which may be written in matrix notation as

$$[\Phi_j^\tau, \Sigma_j^\tau] = \Phi_{j+1}^\tau \mathbf{Q}_j^\tau = \Phi_{j+1}^\tau [\mathbf{Q}_{j,\Phi}^\tau, \mathbf{Q}_{j,\Sigma}^\tau]. \quad (4)$$

To obtain vanishing moments and orthonormality, the transform  $\mathbf{Q}_j^\tau$  is derived from an orthogonal decomposition of the *moment matrix*  $\mathbf{M}_{j+1}^\tau \in \mathbb{R}^{m_q \times n_{j+1}^\tau}$ , given by

$$\mathbf{M}_{j+1}^\tau := \begin{bmatrix} (\mathbf{x}^0, \varphi_{j+1,1})_\Omega & \cdots & (\mathbf{x}^0, \varphi_{j+1,n_{j+1}^\tau})_\Omega \\ \vdots & & \vdots \\ (\mathbf{x}^\alpha, \varphi_{j+1,1})_\Omega & \cdots & (\mathbf{x}^\alpha, \varphi_{j+1,n_{j+1}^\tau})_\Omega \end{bmatrix} = [(\mathbf{x}^\alpha, \Phi_{j+1}^\tau)_\Omega]_{|\alpha| \leq q}.$$

Herein,  $m_q$  is given as in (3) and denotes the dimension of the space  $\mathcal{P}_q(\Omega)$  of total degree polynomials.

In the original construction by Tausch and White, the matrix  $\mathbf{Q}_j^\tau$  is obtained from the singular value decomposition of  $\mathbf{M}_{j+1}^\tau$ . For the construction of samplers, we follow the idea from [1] and rather employ the QR decomposition, which results in samplers with an increasing number of vanishing moments. We compute

$$(\mathbf{M}_{j+1}^\tau)^\top = \mathbf{Q}_j^\tau \mathbf{R} =: [\mathbf{Q}_{j,\Phi}^\tau, \mathbf{Q}_{j,\Sigma}^\tau] \mathbf{R} \quad (5)$$

The moment matrix for the cluster's scaling distributions and samplers is now given by

$$\begin{aligned}
 [\mathbf{M}_{j,\Phi}^\tau, \mathbf{M}_{j,\Sigma}^\tau] &= [(\mathbf{x}^\alpha, [\Phi_j^\tau, \Sigma_j^\tau])_\Omega]_{|\alpha| \leq q} \\
 &= [(\mathbf{x}^\alpha, \Phi_{j+1}^\tau [\mathcal{Q}_{j,\Phi}^\tau, \mathcal{Q}_{j,\Sigma}^\tau])_\Omega]_{|\alpha| \leq q} \\
 &= \mathbf{M}_{j+1}^\tau [\mathcal{Q}_{j,\Phi}^\tau, \mathcal{Q}_{j,\Sigma}^\tau] \\
 &= \mathbf{R}^\top.
 \end{aligned}$$

Since  $\mathbf{R}^\top$  is a lower triangular matrix, the first  $k-1$  entries in its  $k$ -th column are zero. This amounts to  $k-1$  vanishing moments for the  $k$ -th distribution generated by the orthogonal transform  $\mathcal{Q}_j^\tau = [\mathcal{Q}_{j,\Phi}^\tau, \mathcal{Q}_{j,\Sigma}^\tau]$ . Defining the first  $m_q$  distributions as scaling distributions and the remaining ones as samplers, we obtain samplers with vanishing moments at least of order  $q+1$ .

The orthogonality of basis elements of two different clusters results from the non-overlapping supports, while orthogonality within a given branch is a consequence of the orthogonality of the transforms. A visualization of a scaling distribution and samplers on levels  $j=1$  and  $j=2$  with  $q+1=3$  vanishing moments on  $N=200$  uniformly distributed data sites is shown in Figure 1.

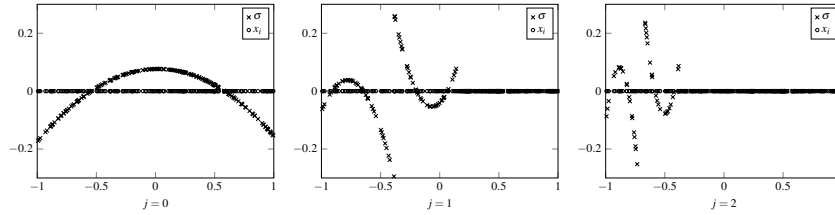


**Fig. 1** Scaling distribution (left), sampler on level  $j=1$  (middle) and sampler on level  $j=2$  (right) for  $N=200$  uniformly distributed data sites and  $q+1=3$ .

If we choose a minimum leaf size  $|\tau| \geq m_{\hat{q}} \geq 2m_q$  for the cluster tree for some polynomial degree  $\hat{q} > q$ , we can even construct samplers whose number of vanishing moments increase successively from order  $q+1$  up to order  $\hat{q}+1$  without additional cost. This is advantageous since more vanishing moments typically improve the a-posteriori compression ratios of a given signal. Moreover, the preceding algebraic construction (5) of vanishing moments can easily be adapted to other primitives, for example, anisotropic total degree polynomial spaces. This particularly makes sense in the higher dimensional setting, when dimension weights are available.

*Remark 2.* Each cluster has at most a constant number of scaling distributions and samplers. For leaf clusters, this number is bounded by the leaf size. For non-leaf clusters, it is bounded by the number of scaling distributions from its child clusters. As there are two child clusters with a maximum of  $m_q$  scaling distributions each, we obtain the bound  $2m_q$  for non-leaf clusters. If the cluster tree is balanced, resulting

in a leaf size of  $\mathcal{O}(1)$ , the above construction of the samplet basis has hence cost  $\mathcal{O}(N)$ .

For leaf clusters, we define the scaling distributions by the Dirac measures supported at the points  $\mathbf{x}_i$ , viz.,  $\Phi^\tau := \{\delta_{\mathbf{x}_i} : \mathbf{x}_i \in \tau, \tau \in \mathcal{L}(\mathcal{T})\}$ . The scaling distributions of all clusters on a specific level  $j$  then generate the spaces

$$\mathcal{X}_j := \text{span}\{\varphi_{j,k}^\tau : k \in I_j^{\Phi,\tau}, \text{level}(\tau) = j\}. \quad (6)$$

In contrast, the samplets span the detail spaces

$$\mathcal{S}_j := \text{span}\{\sigma_{j,k}^\tau : k \in I_j^{\Sigma,\tau}, \text{level}(\tau) = j\}. \quad (7)$$

Combining the scaling distributions of the root cluster with all clusters' samplets gives rise to the samplet basis

$$\Sigma := \Phi^X \cup \bigcup_{\tau \in \mathcal{T}} \Sigma^\tau. \quad (8)$$

## 2.4 Properties of the samplets

The properties of the samplet basis constructed in the previous paragraph are summarized in the next theorem, which can be inferred by adapting the corresponding results from [39, 71].

**Theorem 1.** *The spaces  $\mathcal{X}_j$  defined in equation (6) form a multiresolution analysis*

$$\mathcal{X}_0 \subset \mathcal{X}_1 \subset \dots \subset \mathcal{X}_J = \mathcal{X},$$

where the respective complement spaces  $\mathcal{S}_j$  from (7) satisfy

$$\mathcal{X}_{j+1} = \mathcal{X}_j \oplus^\perp \mathcal{S}_j \text{ for all } j = 0, 1, \dots, J-1.$$

The associated samplet basis  $\Sigma$  defined in (8) is an orthonormal basis in  $\mathcal{X}$ . In particular, there holds:

- (i) The number of all samplets on level  $j$  behaves like  $2^j$ .
- (ii) The samplets have  $q+1$  vanishing moments.
- (iii) Each samplet is supported in a specific cluster  $\tau$ .

The key for data compression and feature detection is the following estimate which shows that the samplet coefficients decay with respect to the samplet's support size provided that the data result from the evaluation of a smooth function on the samplet's support, compare [41].

**Lemma 1.** *Given a sampler  $\sigma_{j,k}$  with support  $\tau$  and let  $f \in C(\Omega)$  with  $f \in C^{q+1}(\Omega)$  for any open set  $\Omega \supset \tau$ . Then, there holds*

$$|(f, \sigma_{j,k})_{\Omega}| \leq \sqrt{|\tau|} \left(\frac{d}{2}\right)^{q+1} \frac{\text{diam}(\tau)^{q+1}}{(q+1)!} \|f\|_{C^{q+1}(\Omega)}.$$

Hence, in case of smooth data, the sampler coefficients are small and can be set to zero without compromising the accuracy. Vice versa, a large sampler coefficient indicates that the data are singular in the region of the sampler's support. If the set  $X$  is *quasi-uniform* in the sense that the *separation radius*  $q_X := \min_{i \neq j} \|\mathbf{x}_i - \mathbf{x}_j\|_2$  and the *fill distance*  $h_{X,\Omega} := \sup_{\mathbf{x} \in \Omega} \min_{\mathbf{x}_i \in X} \|\mathbf{x} - \mathbf{x}_i\|_2$  satisfy  $q_X \sim h_{X,\Omega}$ , then there holds  $\text{diam}(\tau) \sim 2^{-\text{level}(\tau)/d}$ . In this case, Lemma 1 even guarantees the exponential decay of the sampler coefficients with the level provided that the underlying signal is smooth.

### 3 Scattered data analysis

#### 3.1 Fast sampler transform

To transform between the sampler basis and the basis of Dirac measures, we introduce the *fast sampler transform* and its inverse. In accordance with [71], this transform and its inverse can be performed in linear cost. This result is well-known in case of wavelets and was crucial for their rapid development.

The mapping  $f \mapsto [(f, \delta_{\mathbf{x}_1})_{\Omega}, \dots, (f, \delta_{\mathbf{x}_N})_{\Omega}]^{\top}$  defines an operator  $I: C(\Omega) \rightarrow \mathbb{R}^N$ , called *information operator* in the context of optimal recovery, see [59]. By employing samplers, this information is represented in a multiresolution fashion  $f \mapsto [(f, \sigma_{j,k})_{\Omega}]_{j,k}^{\top} \in \mathbb{R}^N$ . More precisely, letting

$$\mathbf{f}^{\Delta} := If \quad \text{and} \quad \mathbf{f}^{\Sigma} := [(f, \sigma_{j,k})_{\Omega}]^{\top}, \quad (9)$$

the fast sampler transform computes

$$\mathbf{f}^{\Sigma} = \mathbf{T} \mathbf{f}^{\Delta},$$

where  $\mathbf{T} \in \mathbb{R}^{N \times N}$  is the orthogonal matrix containing the expansion coefficients of the sampler basis.

The actual implementation of the fast sampler transform is recursive and follows the fishbone scheme of the fast wavelet transform, see Figure 2 for a respective illustration of this scheme. The underlying recursion is based on the refinement relation (4), which translates to

$$(f, [\Phi_j^{\tau}, \Sigma_j^{\tau}])_{\Omega} = (f, \Phi_{j+1}^{\tau} [\mathcal{Q}_{j,\Phi}^{\tau}, \mathcal{Q}_{j,\Sigma}^{\tau}])_{\Omega} = (f, \Phi_{j+1}^{\tau})_{\Omega} [\mathcal{Q}_{j,\Phi}^{\tau}, \mathcal{Q}_{j,\Sigma}^{\tau}]. \quad (10)$$

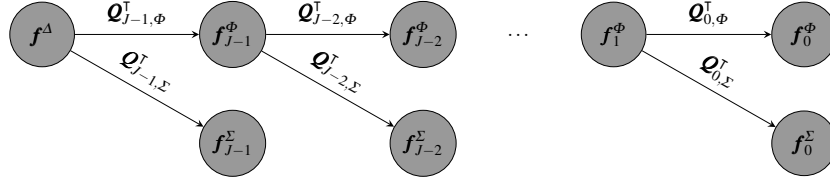


**Fig. 2** Fishbone scheme of the fast samplet transform.

On the finest level, the entries of the vector  $(f, \Phi_j^\tau)_\Omega$  are exactly those of  $\mathbf{f}^\Delta$ . Recursive application of (10) therefore yields all the coefficients  $(f, \Sigma_j^\tau)_\Omega$ , including  $(f, \Phi_0^X)_\Omega$ , required for the representation of  $\mathbf{f}^\Delta$  in the samplet basis.

The inverse transform is obtained in complete analogy by reversing the steps of the fast samplet transform: For each cluster, we compute

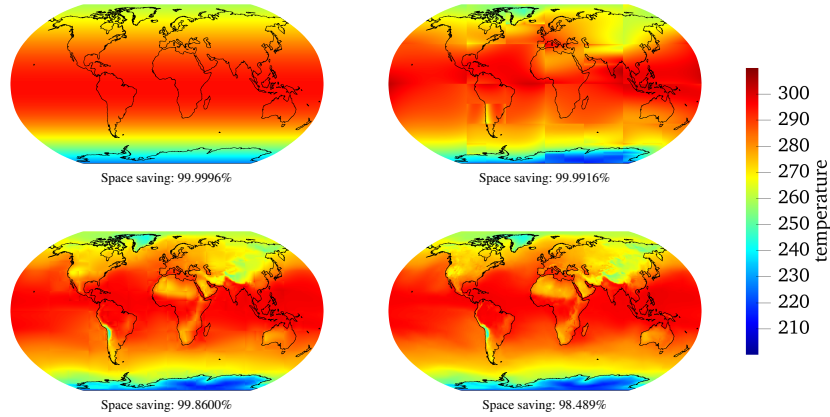
$$(f, \Phi_{j+1}^\tau)_\Omega = (f, [\Phi_j^\tau, \Sigma_j^\tau])_\Omega [\mathbf{Q}_{j,\Phi}^\tau, \mathbf{Q}_{j,\Sigma}^\tau]^\top$$

to either obtain the coefficients of the child clusters' scaling distributions or, for leaf clusters, the coefficients  $\mathbf{f}^\Delta$ .

### 3.2 Data compression

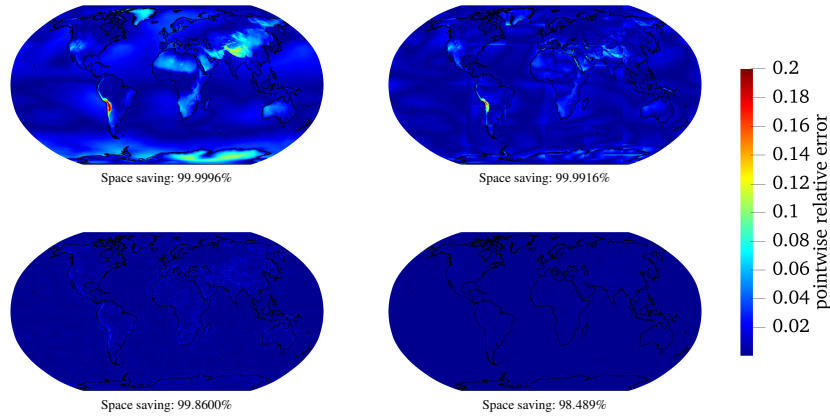
In view of Lemma 1, samplets enable data compression by means of so-called *hard-thresholding*. Given the coefficients  $\mathbf{f}^\Sigma$  of a transformed signal, we define  $\text{HT}_w(\mathbf{f}^\Sigma)$  as the operator which sets all entries  $f_i^\Sigma$  with  $|f_i^\Sigma| < w$  to zero. To showcase this application of samplets, we consider the monthly ERA5 temperature data set, which provides the temperature two meters above the earth's surface. ERA5 is a reanalysis by the European Center for Medium-range Weather Forecasts (ECMWF) of global climate and weather for the past eight decades. Data is available from 1940 onwards, see [45]. We use the monthly data from 2022, which comprises, after removing NaN values, 1 038 240 data points per month. This results in 12 458 880 points in total. The original data format is World Geodesic System 1984 (WGS 84), which we transform by using the Robinson projection, see [64], to reduce the distortion and the projection angles. The bounding box for the data is  $[-1.70 \cdot 10^7, 1.70 \cdot 10^7] \times [-8.63 \cdot 10^6, 8.63 \cdot 10^6] \times [0, 11]$ . In particular, the data points are not located on a regular spatial grid and cluster towards the North and South pole. The fill distance with respect to the convex hull of the data points is  $h_{X,\Omega} = 23\,700$  for each time slice, while the separation radius is  $q_X = 7\,260$  for each time slice.

Figure 3 shows the reconstruction  $\mathbf{T}^\top(\text{HT}_w(\mathbf{f}^\Sigma))$  of the hard-thresholded temperature for October 2022 with thresholds  $w = 10^{-k} \|\mathbf{f}\|_2$  for  $k = 2, 3, 4, 5$  and samplets with  $q + 1 = 4$  vanishing moments. The threshold values result in 4, 87, 1454, 15688 non-zero coefficients, which amount to space savings of 99.9996%,



**Fig. 3** Reconstruction of the temperature based on the hard-thresholded coefficient vector for the relative thresholds  $10^{-k}$ ,  $k = 2, 3, 4, 5$  (from top left to bottom right). Notice that in case of  $k = 2$  only the coarse level samplers remain after thresholding.

99.992%, 99.86%, and 98.49%, respectively. The associated relative errors in the Euclidean norm are 2.4%, 1.2%, 0.39%, and 0.11%.



**Fig. 4** Reconstruction error of the temperature with respect to the hard-thresholded coefficient vector for the relative thresholds  $10^{-k}$ ,  $k = 2, 3, 4, 5$  (from top left to bottom right).

The associated pointwise relative errors of the reconstruction are visualized in Figure 4. For the largest threshold, the maximum of the pointwise relative errors is 21%, while it is 2.2% for the smallest threshold.

### 3.3 Adaptive subsampling

Consider data sites  $X = \{\mathbf{x}_1, \dots, \mathbf{x}_N\} \subset \Omega$  and corresponding data values  $\mathbf{f}^\Delta = I\mathbf{f}$ . The cluster tree for  $X$  is denoted by  $\mathcal{T}$  as before. We propose an adaptive subsampling strategy based on the idea of the *adaptive tree approximation* from [7]. Then, given a relevant subtree, we pursue an *entropy based approach* for sampling uniformly from the leaves of that subtree.

We start by generating a suitable subtree of  $\mathcal{T}$  from the transformed data values  $\mathbf{f}^\Sigma = \mathbf{T}\mathbf{f}^\Delta$ . To this end, we apply tree-coarsening as developed in [7] and directly adapt it to our setting. The *energy* contained in a cluster  $\tau \in \mathcal{T}$  is defined as the sum of energies of its children plus the squared Euclidean norm of the sample coefficients belonging to  $\tau$ , viz.,

$$e(\tau) := \sum_{\tau' \in \text{child}(\tau)} e(\tau') + \sum_{\sigma \in \Sigma^\tau} (f, \sigma)_\Omega^2. \quad (11)$$

Herein, we made the convention that  $\Sigma^X$  also contains the scaling distributions the coarsest level. The quantity  $e(\tau)$  is the contribution of the subtree with root  $\tau$  to the squared norm  $\|\mathbf{f}^\Sigma\|_2^2$ . In particular, we have  $e(X) = \|\mathbf{f}^\Sigma\|_2^2$ .

Based on the energies (11), we next define

$$\tilde{e}(\tau') := q(\tau) := \frac{\sum_{\mu \in \text{child}(\tau)} e(\mu)}{e(\tau) + \tilde{e}(\tau)} \tilde{e}(\tau) \text{ for all } \tau' \in \text{child}(\tau),$$

where we set  $\tilde{e}(X) := e(X)$  for the root of the cluster tree. Given this modified energy, we perform the thresholding version of the second algorithm from [7] with threshold  $w = \varepsilon^2 \|\mathbf{f}^\Sigma\|_2^2$ . This results in a subtree  $\mathcal{T}_w$  that approximates  $\mathbf{f}^\Sigma$  up to a relative error of  $\varepsilon$  in the Euclidean norm. Since the algorithm always selects either none or all children of a given cluster,  $\mathcal{T}_w$  is a cluster tree and its leaves  $\mathcal{L}(\mathcal{T}_w)$  form a partition of  $X$ .

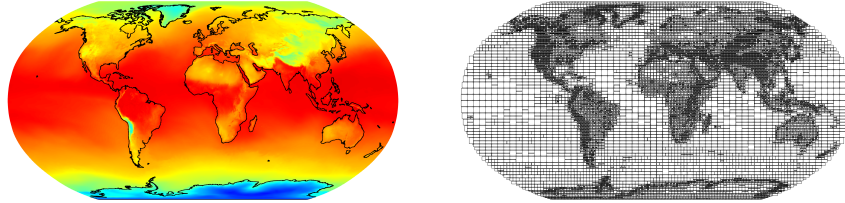


**Fig. 5** Average temperature in October 2022 (left) and leaves of the corresponding adaptive tree with relative threshold  $\varepsilon = 10^{-4}$  (right).

Given the partition generated by  $\mathcal{L}(\mathcal{T}_w)$ , we intend to generate a subsample  $(\mathbf{x}_{i_j}, f_{i_j})$ ,  $j = 1, \dots, n \leq N$ , adapted to the features of the data. To this end, we pursue



an *entropy based approach*: Let  $\mathbb{P}$  be a probability distribution on a discrete finite set  $Z$ . Then, the *information content* of a sample  $z \in Z$  is defined as  $I_{\mathbb{P}}(z) := -\log \mathbb{P}(z)$ . The *entropy*  $H_{\mathbb{P}}$  is the expected information content

$$H_{\mathbb{P}} := \mathbb{E}_{\mathbb{P}}[I_{\mathbb{P}}] = - \sum_{z \in Z} \mathbb{P}(z) \log \mathbb{P}(z). \quad (12)$$

It is well-known that the entropy (12) is maximized if each element of  $Z$  is chosen with the same probability

$$\mathbb{P}(z) = \frac{1}{|Z|},$$

see the seminal work [69] for all the details. Therefore, to generate the adaptive subsample, we shall maximize the entropy for randomly selecting points from leafs by choosing a point  $\mathbf{x} \in X$  from a certain leaf  $\tau \in \mathcal{L}(\mathcal{T}_w)$  with probability

$$\mathbb{P}(\mathbf{x} \in \tau) = \frac{1}{|\mathcal{L}(\mathcal{T}_w)|}. \quad (13)$$

We like to emphasize that (13) can also be used to adaptively generate new samples  $\mathbf{x} \in \Omega$  instead of considering only available points  $\mathbf{x} \in X$ .

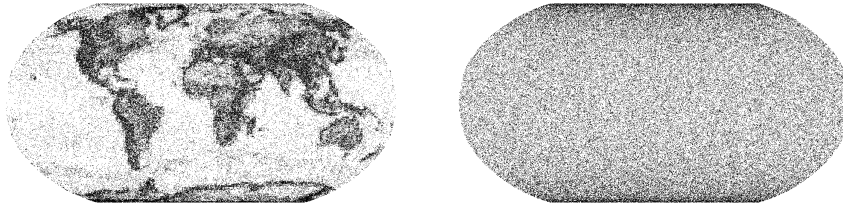


**Fig. 6** Adaptive random subsample (left) and uniform random subsample (right).

To demonstrate the adaptive subsampling approach, we consider again the ERA5 temperature data set. Tree coarsening with relative threshold  $\varepsilon = 10^{-4}$  for samplers with  $q + 1 = 4$  vanishing moments yields the tree found in the right plot of Figure 5. The associated data are visualized in the accompanying left plot. The result of the subsampling using 100 000 points for the month October yields the point distribution seen in the left plot of Figure 6. In contrast, using the same amount of uniformly distributed samples yields the distribution in the right plot of Figure 6.

## 4 Scattered data approximation

### 4.1 Reproducing kernel Hilbert spaces

Let  $\mathcal{H} \subset C(\Omega)$  be a Hilbert space with inner product  $\langle \cdot, \cdot \rangle_{\mathcal{H}}$ . Then, there holds  $\delta_{\mathbf{x}} \in \mathcal{H}'$  for every  $\mathbf{x} \in \Omega$ . Consequently, by the Riesz representation theorem, there exists  $(R\delta_{\mathbf{x}}) \in \mathcal{H}$  such that

$$\langle (R\delta_{\mathbf{x}}), f \rangle_{\mathcal{H}} = f(\mathbf{x}) \text{ for all } f \in \mathcal{H}. \quad (14)$$

The function  $\kappa(\mathbf{x}, \mathbf{y}) := (R\delta_{\mathbf{x}})(\mathbf{y})$  is the *reproducing kernel* for  $\mathcal{H}$ , which renders it a *reproducing kernel Hilbert space*, see [3, 76] for instance. Especially, the reproducing kernel is symmetric and positive definite in the following sense.

**Definition 3.** A symmetric kernel  $\kappa: \Omega \times \Omega \rightarrow \mathbb{R}$  is *positive definite* on  $\Omega \subset \mathbb{R}^d$ , iff the *kernel matrix*  $\mathbf{K} := [\kappa(\mathbf{x}_i, \mathbf{x}_j)]_{i,j=1}^N$  is symmetric and positive semi-definite for every choice of mutually distinct points  $\mathbf{x}_1, \dots, \mathbf{x}_N \in \Omega$  and any  $N \in \mathbb{N}$ . The kernel  $\kappa$  is *strictly positive definite*, iff  $\mathbf{K}$  is even positive definite.

Associated to  $X = \{\mathbf{x}_1, \dots, \mathbf{x}_N\} \subset \Omega$ , we introduce the subspace of kernel translates

$$\mathcal{H}_X := \text{span}\{\phi_1, \dots, \phi_N\} \subset \mathcal{H}, \quad (15)$$

where

$$\phi_i := \kappa(\mathbf{x}_i, \cdot) \text{ for } i = 1, \dots, N.$$

The subspace  $\mathcal{H}_X$  is isometrically isomorphic to  $\mathcal{X} = \text{span}\{\delta_{\mathbf{x}_1}, \dots, \delta_{\mathbf{x}_N}\} \subset \mathcal{H}'$  by the Riesz isometry. We identify

$$u' = \sum_{i=1}^N u_i \delta_{\mathbf{x}_i} \in \mathcal{X}$$

with

$$Ru = \sum_{i=1}^N u_i \phi_i \in \mathcal{H}_X.$$

To approximate a general element  $h \in \mathcal{H}$  by an element in  $\mathcal{H}_X$ , we compute its orthogonal projection. The latter is obtained by the solution of the Galerkin formulation

$$\langle s_h, v \rangle_{\mathcal{H}} = \langle h, v \rangle_{\mathcal{H}} \text{ for all } v \in \mathcal{H}_X. \quad (16)$$

Making the ansatz

$$s_h = \sum_{i=1}^N \alpha_i \phi_i \quad (17)$$

and choosing the basis of kernel translates as test functions in (16), we arrive at the equivalent interpolation problem  $s_h(\mathbf{x}_i) = h(\mathbf{x}_i)$  for all  $\mathbf{x}_i \in X$  due to the reproducing

property (14). The expansion coefficients  $\boldsymbol{\alpha} = [\alpha_i]_{i=1}^N$  from (17) can be retrieved by solving the linear system of equations

$$\mathbf{K}\boldsymbol{\alpha} = \mathbf{h}, \text{ where } \mathbf{h} := Ih = [(h, \delta_{\mathbf{x}_i})_{\Omega}]_{i=1}^N, \quad (18)$$

Here,  $\mathbf{K} = [\kappa(\mathbf{x}_i, \mathbf{x}_j)]_{i,j=1}^N$  is the kernel matrix and  $I$  is the information operator from (9). It is known from both, Galerkin theory and optimal recovery, that  $s_h$  is a minimum norm solution in  $\mathcal{H}$ , see [10] and [58], respectively.

Depending on the choice of the kernel function, the linear system (18) of equations can be ill conditioned and a suitable regularization is required to obtain a solution. Traditionally, Tikhinov regularization is used and the system

$$(\mathbf{K} + \mu \mathbf{I})\boldsymbol{\alpha} = \mathbf{h} \quad (19)$$

is solved for an appropriate regularization parameter  $\mu > 0$ . In Section 4.7, we address also  $\ell^1$ -regularization with respect to the samplet basis, which is known to impose sparsity to the solution.

## 4.2 Samplers in reproducing kernel Hilbert spaces

Employing the Riesz isometry, we can embed a given samplet basis  $\boldsymbol{\Sigma} = \{\sigma_{j,k}\}_{j,k}$  into a reproducing kernel Hilbert space. This idea follows the vast literature on the embedding of empirical distributions into reproducing kernel Hilbert spaces, see [60] for example.

Consider a samplet

$$\sigma_{j,k} = \sum_{i=1}^N \omega_{j,k,i} \delta_{\mathbf{x}_i} \in \mathcal{H}'$$

where  $\omega_{j,k,i}$ ,  $i = 1, \dots, N$ , are the expansion coefficients of  $\sigma_{j,k}$  with respect to the Dirac- $\delta$ -distributions in  $\mathcal{X}$ . The samplet can be identified with the function

$$\psi_{j,k} := \sum_{i=1}^N \omega_{j,k,i} \phi_i \in \mathcal{H}$$

by means of the Riesz isometry. The vanishing moment property (2) translates to

$$\langle \psi_{j,k}, h \rangle_{\mathcal{H}} = 0$$

for any  $h \in \mathcal{H}$  which satisfies  $h|_O \in \mathcal{P}_q$  for any open and convex set  $O$  with  $\text{supp}(\sigma_{j,k}) \subset O \cap \Omega$ . Herein, we define the support of a samplet in the context of the support of measures according to

$$\text{supp}(\sigma_{j,k}) := \{\mathbf{x}_i \in X : \omega_{j,k,i} \neq 0\}.$$

The functions  $\{\psi_{j,k}\}_{j,k}$  span the subspace  $\mathcal{H}_X$ , see (15). In particular, defining

$$\mathcal{W}_j := \text{span}\{\psi_{j,k}\}_k,$$

we obtain the primal multiresolution analysis

$$\mathcal{H}_X = \bigoplus_j \mathcal{W}_j.$$

Using the embedded samplers  $\psi_{j,k}$  as ansatz- and test functions in the Galerkin formulation (16) yields the linear system of equations

$$\mathbf{K}^\Sigma \boldsymbol{\beta} = \mathbf{h}^\Sigma, \quad (20)$$

where

$$\begin{aligned} \mathbf{K}^\Sigma &= [(\kappa, \sigma_{j,k} \otimes \sigma_{j',k'})_{\Omega \times \Omega}]_{j,j',k,k'} \\ &= [\langle \psi_{j,k}, \psi_{j',k'} \rangle_{\mathcal{H}}]_{j,j',k,k'} \\ &= \mathbf{T} \mathbf{K} \mathbf{T}^\top \end{aligned} \quad (21)$$

and

$$\mathbf{h}^\Sigma = [(\sigma_{j,k}, h)_\Omega]_{j,k} = [\langle \psi_{j,k}, h \rangle_{\mathcal{H}}]_{j,k} = \mathbf{T} \mathbf{h}.$$

The solution  $\boldsymbol{\beta}$  of the linear system (20) of equations is equivalent to the one of (18) by the transform

$$\boldsymbol{\beta} = \mathbf{T} \boldsymbol{\alpha} = \mathbf{T} \mathbf{K}^{-1} \mathbf{h}.$$

Noticing that the Gramian satisfies

$$[\langle \kappa(\mathbf{x}_i, \cdot), \kappa(\mathbf{x}_j, \cdot) \rangle_{\mathcal{H}}]_{i,j=1}^N = [\kappa(\mathbf{x}_i, \mathbf{x}_j)]_{i,j=1}^N = \mathbf{K},$$

we find

$$\langle \psi_{j,k}, \psi_{j',k'} \rangle_{\mathcal{H}} = \boldsymbol{\omega}_{j,k}^\top \mathbf{K} \boldsymbol{\omega}_{j',k'},$$

where we set  $\boldsymbol{\omega}_{j,k} := [\omega_{j,k,i}]_{i=1}^N$  and  $\boldsymbol{\omega}_{j',k'} := [\omega_{j',k',i}]_{i=1}^N$ . Hence, the *dual basis* is given by

$$\tilde{\psi}_{j,k} = \sum_{i=1}^N \tilde{s}_{j,k,i} \phi_i, \quad \text{where } \tilde{\boldsymbol{\omega}}_{j,k} := \mathbf{K}^{-1} \boldsymbol{\omega}_{j,k}.$$

Defining the spaces

$$\tilde{\mathcal{W}}_j := \text{span}\{\tilde{\psi}_{j,k}\}_k$$

yields the dual multiresolution analysis

$$\mathcal{H}_X = \bigoplus_j \tilde{\mathcal{W}}_j,$$

where  $\mathcal{W}_j \perp \tilde{\mathcal{W}}_{j'}$  for  $j \neq j'$  since  $\langle \psi_{j,k}, \tilde{\psi}_{j',k'} \rangle_{\mathcal{H}} = \delta_{j,j'} \delta_{k,k'}$ .

With respect to the dual basis, the interpolant (17) can be written as

$$s_h = \sum_{j,k} \beta_{j,k} \psi_{j,k} = \sum_{j,k} \langle \tilde{\psi}_{j,k}, h \rangle_{\mathcal{H}} \psi_{j,k} = \sum_{j,k} \langle \psi_{j,k}, h \rangle_{\mathcal{H}} \tilde{\psi}_{j,k}. \quad (22)$$

In view of the multiresolution representation of the information operator in  $Ih = [(h, \sigma_{j,k})_\Omega]_{j,k} = [\langle h, \psi_{j,k} \rangle_{\mathcal{H}}]_{j,k}$ , compare (9), the expansion with respect to the dual basis in (22) amounts to the multiresolution variant of the optimal recovery algorithm from [59].

In order to give a visual idea of such *embedded samplers* and the respective dual basis, we consider the Sobolev space  $H^1(\mathbb{R})$ , equipped with the usual norm

$$\|u\|_{H^1(\mathbb{R})}^2 = \|u\|_{L^2(\mathbb{R})}^2 + \|u'\|_{L^2(\mathbb{R})}^2.$$

Its reproducing kernel is given by  $\kappa(s, t) = \frac{1}{2} \exp(|s - t|)$ , see [5] for instance. Figure 7 shows an embedded scaling distribution (left plot) and two embedded samplers (middle and right plots) with  $q + 1 = 3$  vanishing moments, constructed for  $N = 200$  uniformly distributed data sites.

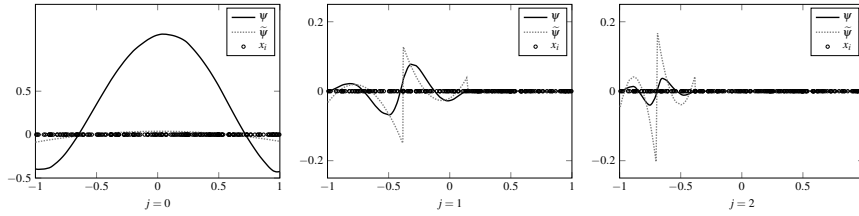


**Fig. 7**  $H^1(\mathbb{R})$ -embedded primal and dual scaling distribution (left), sampler on level  $j = 1$  (middle) and sampler on level  $j = 2$  (right) for  $N = 200$  uniformly distributed data sites and  $q + 1 = 3$ .

### 4.3 Asymptotically smooth kernels

It is well-known that nonlocal operators of Calderón-Zygmund type can be compressed in wavelet coordinates, see [6, 21, 67, 74, 75] for example. Analogous results are available for samplers in the context of kernel matrices of positive definite kernels.

The essential ingredient for the sampler compression of kernel matrices is the *asymptotical smoothness* property of the kernel  $\kappa$ . This means that there exists a  $\rho > 0$  such that for all  $(\mathbf{x}, \mathbf{y}) \in (\Omega \times \Omega) \setminus \Delta$

$$\left| \frac{\partial^{|\alpha|+|\beta|}}{\partial \mathbf{x}^\alpha \partial \mathbf{y}^\beta} \kappa(\mathbf{x}, \mathbf{y}) \right| \lesssim \frac{(|\alpha| + |\beta|)!}{\rho^{|\alpha|+|\beta|} \|\mathbf{x} - \mathbf{y}\|_2^{|\alpha|+|\beta|}} \quad (23)$$

uniformly in  $\alpha, \beta \in \mathbb{N}^d$  apart from the diagonal  $\Delta := \{(\mathbf{x}, \mathbf{y}) \in \Omega \times \Omega : \mathbf{x} = \mathbf{y}\}$ .

A particular class of positive definite kernels which are asymptotically smooth are the *Matérn kernels*  $\kappa(\mathbf{x}, \mathbf{y}) := k_\nu(\|\mathbf{x} - \mathbf{y}\|_2)$ . They are known to be the reproduc-

ing kernels of the Sobolev spaces, see [76] for example, and are given by

$$k_\nu(r) := \frac{2^{1-\nu}}{\Gamma(\nu)} \left( \frac{\sqrt{2\nu}r}{\ell} \right)^\nu K_\nu \left( \frac{\sqrt{2\nu}r}{\ell} \right), \quad (24)$$

where  $r = \|\mathbf{x} - \mathbf{y}\|_2 \geq 0$  is the Euclidean distance and  $\ell > 0$  is the lengthscale parameter. Herein,  $K_\nu$  is the modified Bessel function of the second kind of order  $\nu$  and  $\Gamma$  is the gamma function. The parameter  $\nu$  controls the smoothness of the kernel function, see, for example, [77]. In particular, we have the exponential kernel

$$k_{1/2}(r) = \exp \left( -\frac{r}{\ell} \right) \quad (25)$$

and the Gaussian kernel

$$k_\infty(r) = \exp \left( -\frac{r^2}{2\ell^2} \right).$$

For asymptotically smooth kernels, compare (23), we obtain the following result, which is the basis for the matrix compression introduced thereafter. The proof of this result is obtained in the traditional way by applying Taylor's expansion of the kernel function under consideration, using (23) to bound the remainder terms, compare [41].

**Lemma 2.** *Consider two samplers  $\sigma_{j,k}$  and  $\sigma_{j',k'}$  which exhibit  $q+1$  vanishing moments and let the associated clusters  $\tau$  and  $\tau'$  be such that  $\text{dist}(\tau, \tau') > 0$ . Then, for kernels satisfying (23), there holds that*

$$(\kappa, \sigma_{j,k} \otimes \sigma_{j',k'})_{\Omega \times \Omega} \lesssim \sqrt{|\tau||\tau'|} \frac{\text{diam}(\tau)^{q+1} \text{diam}(\tau')^{q+1}}{(\rho \text{dist}(\tau, \tau')/d)^{2(q+1)}}. \quad (26)$$

#### 4.4 Matrix compression

The decay estimate (26) immediately yields a compression strategy for kernel matrices in sampler representation, the proof of which is found in [41]. This compression differs from the wavelet matrix compression introduced in [21], since we do not exploit the decay of the sampler coefficients with respect to the level in case of smooth data. This enables us to also cover scattered data sets with arbitrarily distributed points. As a result, we use the same accuracy on all levels, which is similar to the setting in [6], but implies that the number  $q+1$  of vanishing moments needs to be increased to arrive at a higher accuracy of the matrix compression. Fixing the accuracy seems however not to be an issue in view of the regularization of the kernel matrices in scattered data approximation.

**Theorem 2.** *Set all coefficients of the kernel matrix  $\mathbf{K}^\Sigma$  from (21) to zero which satisfy the admissibility condition*

$$\text{dist}(\tau, \tau') \geq \eta \max\{\text{diam}(\tau), \text{diam}(\tau')\}, \quad \eta > 0, \quad (27)$$

where  $\tau$  is the cluster supporting  $\sigma_{j,k}$  and  $\tau'$  is the cluster supporting  $\sigma_{j',k'}$ , respectively. Then, there holds

$$\|\mathbf{K}^\Sigma - \mathbf{K}_\varepsilon^\Sigma\|_F \lesssim m_q(\rho\eta/d)^{-2(q+1)}N\log(N),$$

where  $m_q$  is given by (3).

*Remark 3.* In case of quasi-uniform points  $\mathbf{x}_i \in X$ , we have  $\|\mathbf{K}^\Sigma\|_F \sim N$ . Moreover, the term  $\log(N)$  can be removed by a refined analysis in this case and we arrive at

$$\frac{\|\mathbf{K}^\Sigma - \mathbf{K}_\varepsilon^\Sigma\|_F}{\|\mathbf{K}^\Sigma\|_F} \lesssim m_q(\rho\eta/d)^{-2(q+1)}$$

while the compressed matrix has  $\mathcal{O}(m_q^2 N \log N)$  nonzero coefficients.

An illustration of the matrix pattern in case of the exponential kernel  $k_{1/2}$  from (25) with lengthscale parameter  $\ell = 0.1$  on the unit square using quasi-uniform samplers with  $q + 1 = 4$  vanishing moments is found in the left plot of Figure 8. Especially, it has been observed in [40] that the compressed matrix can be reordered by means of nested dissection [32] such that a very sparse Cholesky decomposition is obtained. This is illustrated in the middle and right plots of Figure 8.

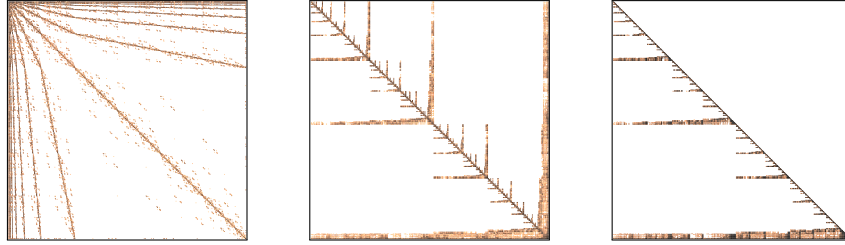


**Fig. 8** Sparsity patterns of the sampler compressed exponential kernel on the unit square (left), the nested dissection reordering (middle), and the Cholesky factor (right). Each dot represents a matrix block of size  $300 \times 300$ . The entries per block are color coded, where lighter blocks have less entries.

#### 4.5 Matrix assembly

Using the compression rule (27), we can now determine for a given pair of clusters whether the corresponding entries need to be calculated. As there are  $\mathcal{O}(N)$  clusters, naively checking the cut-off criterion for all pairs would still take  $\mathcal{O}(N^2)$  operations.

Hence, we require smarter means to determine the non-negligible cluster pairs. For this purpose, we first state the transitivity of the admissibility condition to child clusters, compare [21] for a proof.

**Lemma 3.** *Let  $\tau$  and  $\tau'$  be clusters satisfying the admissibility condition (27). Then, for the child clusters  $\tau_{\text{child}}$  of  $\tau$  and  $\tau'_{\text{child}}$  of  $\tau'$ , we have*

$$\begin{aligned} \text{dist}(\tau, \tau'_{\text{child}}) &\geq \eta \max\{\text{diam}(\tau), \text{diam}(\tau'_{\text{child}})\}, \\ \text{dist}(\tau_{\text{child}}, \tau') &\geq \eta \max\{\text{diam}(\tau_{\text{child}}), \text{diam}(\tau')\}, \\ \text{dist}(\tau_{\text{child}}, \tau'_{\text{child}}) &\geq \eta \max\{\text{diam}(\tau_{\text{child}}), \text{diam}(\tau'_{\text{child}})\}. \end{aligned}$$

The lemma tells us that we may omit cluster pairs whose parent clusters already satisfy the admissibility condition. This is essential for the efficient assembly of the compressed kernel matrix by means of  $\mathcal{H}^2$ -matrix techniques, see [37, 33]. This idea has already been proposed earlier in [1, 39, 50] in case of Tausch-White wavelets.

$\mathcal{H}^2$ -matrices approximate the kernel interaction for sufficiently distant clusters  $\tau$  and  $\tau'$  in the sense of the admissibility condition (27) by means of a polynomial interpolant, see [9]. More precisely, given a suitable set of interpolation points  $\{\xi_t^\tau\}_t$  for each cluster  $\tau$  with associated Lagrange polynomials  $\{\mathcal{L}_t^\tau(\mathbf{x})\}_t$ , we can approximate an admissible matrix block by interpolation:

$$[(\kappa, \delta_{\mathbf{x}} \otimes \delta_{\mathbf{y}})_{\Omega \times \Omega}]_{\mathbf{x} \in \tau, \mathbf{y} \in \tau'} \approx \sum_{s,t} \kappa(\xi_s^\tau, \xi_t^{\tau'}) [(\mathcal{L}_s^\tau, \delta_{\mathbf{x}})_{\Omega}]_{\mathbf{x} \in \tau} [(\mathcal{L}_t^{\tau'}, \delta_{\mathbf{y}})_{\Omega}]_{\mathbf{y} \in \tau'}.$$

However, different from the  $\mathcal{H}^2$ -matrix setting, we shall consider this expansion also when the clusters  $\tau$  and  $\tau'$  are located on different levels of the cluster tree. By running recursively in a clever way through the sample matrix, we arrive at an algorithm scheme that computes the compressed kernel matrix in loglinear overall cost. We skip further details here and refer the reader to [41] instead.

To demonstrate the capabilities of the sample matrix compression, we consider a surface reconstruction problem, similarly to [13]. Given a planar triangulation resulting from a 3D scan of the Laokoon group (the scan is provided by the Statens Museum for Kunst), we generate uniform samples of the signed distance by using the about 500 000 vertices the surface mesh and another 250 000 random points within the bounding box of the Laokoon group. This results in  $N = 750\,000$  data sites in total. The left image in Figure 9 shows a uniform subsample of size 100 000 of the data points. For the interpolation, we consider the exponential kernel  $k_{1/2}$  from (25) with lengthscale parameter  $\ell = 0.01$ , where the data sites are rescaled to the hypercube  $[0, 1]^3$ . The kernel matrix is compressed by using samplelets with  $q + 1 = 4$  vanishing moments and the linear system (19) of equations is solved with the regularization parameter  $\mu = 10^{-8}$  by the conjugate gradient method.

The interpolated signed distance function is then evaluated at a uniform grid of 125 000 000 points, that is 500 points per axis direction. The evaluation is performed by the fast multipole method developed in [42] using total degree polynomials of degree 6 for the interpolation of the kernel function in the farfield. The image in



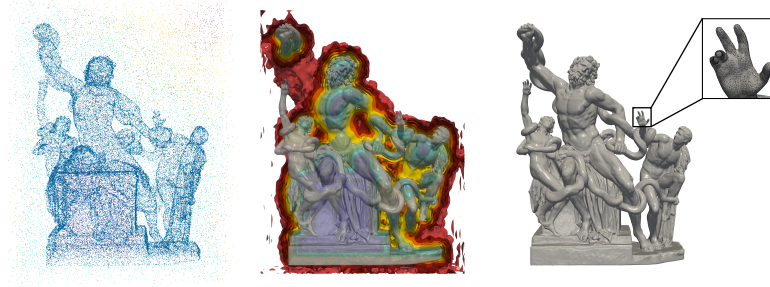


**Fig. 9** Signed distance function interpolation from a surface mesh of the Laokoon group. The left image shows a subsample of the signed distance function used for approximation, the image in the middle shows the levelsets of the signed distance function for the values  $\{-5, -4, \dots, 5\}$ . The image on the right is the zero levelset with a zoom of the original surface mesh and the reconstruction of the right son's left hand.

the middle of Figure 9 shows the levelsets of the signed distance function for the values  $\{-5, -4, \dots, 5\}$ . The right image shows the zero levelset, which corresponds to the desired surface. From the zoom of the right son's hand, it can be seen how the surface is smoothed in comparison to the original surface mesh.

#### 4.6 Multiresolution kernel matrix algebra

Let  $\Omega \subset \mathbb{R}^d$  be a smooth domain and assume that the set of sites  $X \subset \Omega$  is *asymptotically distributed uniformly modulo one*, see [51]. This means, we have for every Riemann integrable function  $f : \Omega \rightarrow \mathbb{R}$  that

$$\left| \int_{\Omega} f(\mathbf{x}) \, d\mathbf{x} - \frac{|\Omega|}{N} \sum_{i=1}^N f(\mathbf{x}_i) \right| \rightarrow 0 \quad \text{as } N \rightarrow \infty.$$

Under this condition, the kernel matrix  $\mathbf{K}$  corresponds to a Nyström discretization of an associated integral operator  $K$ . Namely, the reproducing kernel  $\kappa(\cdot, \cdot)$  gives rise to the compact integral operator

$$K : L^2(\Omega) \rightarrow L^2(\Omega), \quad u \mapsto \int_{\Omega} \kappa(\cdot, \mathbf{y}) u(\mathbf{y}) \, d\mathbf{y}. \quad (28)$$

For many practical applications, (28) constitutes a classical pseudo-differential operator of negative order  $s < 0$ , especially in case of Matérn kernels. We refer to, for example, [48, 65, 68, 72] for the details of this theory, including the subsequent developments. We are interested here in pseudo-differential operators  $K$  which belong to the subclass  $OPS_{cl,1}^s$  of *analytic pseudo-differential operators*, see [65]. Their kernels are known to be asymptotically smooth, satisfying for all  $(\mathbf{x}, \mathbf{y}) \in (\Omega \times \Omega) \setminus \Delta$

the refined decay property

$$\left| \frac{\partial^{|\boldsymbol{\alpha}|+|\boldsymbol{\beta}|}}{\partial \mathbf{x}^{\boldsymbol{\alpha}} \partial \mathbf{y}^{\boldsymbol{\beta}}} \kappa(\mathbf{x}, \mathbf{y}) \right| \lesssim \frac{(|\boldsymbol{\alpha}| + |\boldsymbol{\beta}|)!}{\rho^{|\boldsymbol{\alpha}|+|\boldsymbol{\beta}|} \|\mathbf{x} - \mathbf{y}\|_2^{s+d+|\boldsymbol{\alpha}|+|\boldsymbol{\beta}|}} \quad (29)$$

uniformly in  $\boldsymbol{\alpha}, \boldsymbol{\beta} \in \mathbb{N}^d$ . Note that, in case of reproducing kernels, we always have  $s+d < 0$  due to the continuity of the kernel such that (29) implies also (23), required for the samplet matrix compression in Section 4.4.

The addition  $\mathbf{K} + \mathbf{K}'$  of two compressed kernel matrices in compressed format is obvious. For the computation of the matrix product  $\mathbf{K} \cdot \mathbf{K}'$ , we make use of the fact that it corresponds to the concatenation  $K \circ K'$  of the underlying pseudo-differential operators since

$$\int_{\Omega} \kappa(\mathbf{x}_i, \mathbf{z}) \kappa'(\mathbf{z}, \mathbf{x}_j) d\mathbf{z} \approx \frac{|\Omega|}{N} \sum_{k=1}^N \kappa(\mathbf{x}_i, \mathbf{x}_k) \kappa'(\mathbf{x}_k, \mathbf{x}_j). \quad (30)$$

If  $K \in OPS_{cl,1}^s$  and  $K' \in OPS_{cl,1}^{s'}$ , then there holds  $K \circ K' \in OPS_{cl,1}^{s+s'}$  and, thus,  $K \circ K'$  is compressible. In accordance with [43], we can therefore compute the matrix product  $\mathbf{K}' \cdot \mathbf{K}$  in loglinear complexity on the given matrix pattern.

Consider next a symmetric and positive definite kernel function  $\kappa(\cdot, \cdot)$  such that the associated pseudo-differential operator satisfies  $K \in OPS_{cl,1}^s$  with  $s+d < 0$ . As shown in [43], the inverse of  $K + \mu \text{Id}$  is of the form  $\mu^{-1} \text{Id} - K'$  with  $K'$  being likewise a pseudo-differential operator of class  $OPS_{cl,1}^s$ . Especially, the kernel function  $\kappa'$  which underlies the operator  $K'$  by the Schwartz kernel theorem, see [47] for instance, is symmetric, positive definite, and likewise asymptotically smooth. Thus, the inverse kernel matrix  $(\mathbf{K} + \mu \mathbf{I})^{-1}$  is also compressible and can, in view of (30), be efficiently approximated by selected inversion, see [52], of the associated pattern, see [43] for the details.

More complicated matrix functions like powers of the kernel matrix or the matrix exponential become accessible, too, by using contour integrals, see [38]. Indeed, the kernel matrix algebra proposed in [43] has the property that the arithmetics is exact on the prescribed (fixed) pattern. We refer the reader to [43] for specific examples and results.

## 4.7 Samplet basis pursuit

Sparsity constraints are widely used in computational learning, statistics, and signal processing such as deblurring, feature selection and compressive sensing, see [11, 14, 29, 49, 70] for example. Sparsity constraints are imposed by adding an  $\ell^1$ -penalty term to the functional to be minimized. However, such sparsity constraints make only sense if a basis is used for the discretization where the data become sparse. In the past, mostly wavelets bases, Fourier bases, or frames like curvelets,

contourlets, and shearlets have been used as they are known to give raise to sparse representations, see [12, 26, 28, 31, 36] for example. However, such discretization concepts are based on regular grids and it is not obvious how to extend them to scattered data as they appear often in machine leaning.

In this section, we shall therefore discuss  $\ell^1$ -regularization for scattered data approximation with respect to samplet coordinates. To this end, we consider the functional

$$\min_{\boldsymbol{\alpha} \in \mathbb{R}^N} \frac{1}{2} \|\mathbf{h} - \mathbf{K}\boldsymbol{\alpha}\|_2^2 + \sum_{i=1}^N w_i |\beta_i|, \text{ where } \boldsymbol{\beta} = \mathbf{T}\boldsymbol{\alpha}. \quad (31)$$

The weight vector  $\mathbf{w} = [w_i]_i \in \mathbb{R}^N$  plays the role of the regularization parameter, where each coefficient is regularized individually. We refer to, e.g., [26, 53, 63] for the analysis of the regularizing properties and for appropriate parameter choice rules.

Numerical algorithms to solve the optimization problem (31) are based on soft-thresholding. Indeed, the sparsity constrained minimization problem (31) can be recast into the root finding problem

$$\mathbf{0} = \boldsymbol{\beta}^* - \text{SS}_{\boldsymbol{w}}(\boldsymbol{\beta}^* + \gamma(\mathbf{K}^\Sigma)^\top(\mathbf{h}^\Sigma - \mathbf{K}^\Sigma \boldsymbol{\beta}^*)), \quad (32)$$

where  $\gamma > 0$  and

$$\text{SS}_{\boldsymbol{w}}(\mathbf{v}) := \text{sign}(\mathbf{v}) \max\{\mathbf{0}, |\mathbf{v}| - \mathbf{w}\}$$

is the soft-shrinkage operator. Problem (32) can efficiently be solved by the semi-smooth Newton method, see [4, 34].

In the spirit of [15, 35], also a dictionary of multiple kernels can be employed in (31). Given the kernels  $\kappa_1, \dots, \kappa_L$ , we are then looking for a sparse representation of the form

$$s_h = \sum_{\ell=1}^L \sum_{i=1}^N \alpha_i^{(\ell)} \kappa_\ell(\mathbf{x}_i, \cdot) = \sum_{\ell=1}^L \sum_{i=1}^N \beta_i^{(\ell)} \psi_i^{(\ell)}.$$

Setting

$$\mathbf{K} := [\mathbf{K}_1, \dots, \mathbf{K}_L], \quad \mathbf{K}_\ell := [\kappa_\ell(\mathbf{x}_i, \mathbf{x}_j)]_{i,j=1}^N,$$

and

$$\boldsymbol{\alpha}^\top := [\boldsymbol{\alpha}_1^\top, \dots, \boldsymbol{\alpha}_L^\top], \quad \boldsymbol{\alpha}_j \in \mathbb{R}^N,$$

this approach also amounts to (31) with obvious modifications. The most important difference to the original problem is, of course, that the matrix  $\mathbf{K}$  is not quadratic any more. This means that the underlying linear system  $\mathbf{K}\boldsymbol{\alpha} = \mathbf{h}$  of equations is underdetermined.

To illustrate the approach, we consider the sparse reconstruction of the temperature data from the ERA5 data set in space-time. We employ two space-time kernels, namely

$$\kappa_1(\mathbf{z}, \mathbf{z}') := k_{3/2}(\|\mathbf{x} - \mathbf{y}\|_2) k_{\text{per}}(|t - t'|)$$

and

$$\kappa_2(\mathbf{z}, \mathbf{z}') := k_{1/2}(\|\mathbf{z} - \mathbf{z}'\|_2),$$

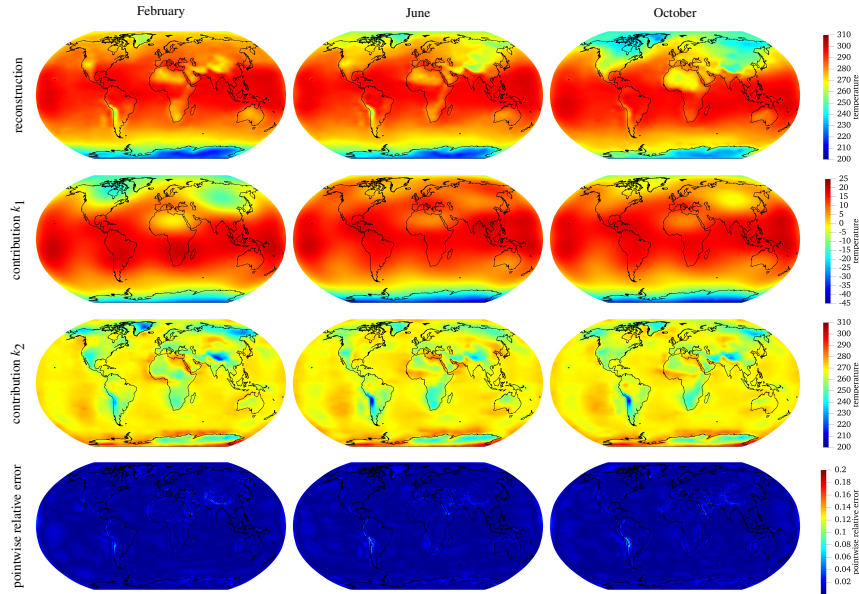


**Fig. 10** Reconstruction of the average temperature for February, June, October 2022 (top row), contributions of  $k_1, k_2$  (second and third row) and pointwise relative error (bottom row).

where  $\mathbf{z} := (\mathbf{x}, t)$  and  $\mathbf{z}' := (\mathbf{y}, t')$ . Herein, the lengthscale parameter is set to  $\ell = 0.2$  for  $k_{3/2}$  and to  $\ell = 0.01$  for  $k_{1/2}$ , compare (24). Moreover, we define the periodic Gaussian kernel  $k_{\text{per}}(r) := e^{-50 \sin^2(\pi r)}$ . The kernel  $\kappa_1$  is a tensor product kernel with relatively large lengthscale parameter. This kernel is intended to capture the smooth parts of the temperature distribution over time. The second kernel  $\kappa_2$  is a quite rough exponential kernel in space time and chosen to capture sharp features.

For the numerical computation, the set of data sites is obtained by adaptively sampling 100000 data sites per time step, compare Section 3.3. This results in  $N = 1200000$  data sites in total. These data sites are rescaled to the unit hypercube  $[0, 1]^3$ . For the compression of the respective kernel matrices, we apply samplers with  $q + 1 = 4$  vanishing moments. We compute the coefficients in (31) by using an iteratively regularized version of the semi-smooth Newton method, see [4] for details. The weight vector  $\mathbf{w}$  is set to  $w_i = 10^{-6}$  for all  $i = 1, \dots, N$ . We obtain  $\|\boldsymbol{\beta}_1\|_0 = 671$  and  $\|\boldsymbol{\beta}_2\|_0 = 5883$  non-vanishing coefficients, resulting in a relative in-sample error of  $8.18 \cdot 10^{-3}$  in the Euclidean norm, while the value of the functional is  $4.76 \cdot 10^{-5}$ . The pointwise relative error which is obtained on the full data set is smaller than 9.73% for all time steps.

The top row of Figure 10 shows the reconstruction evaluated for the full data set for the months February, June, and October. The second row shows the contribution of  $\kappa_1$ . As can be seen,  $\kappa_1$  captures the coarse-scale structure of the temperature distribution with relatively few coefficients. The third row shows the contribution

of  $\kappa_2$ . The kernel localizes at the coast lines and mountains and represents sharp features, which requires the major part of the non-zero coefficients. The pointwise relative approximation error is finally found in the last row.

## References

1. D. Alm, H. Harbrecht, and U. Krämer. The  $\mathcal{H}^2$ -wavelet method. *J. Comput. Appl. Math.*, 267:131–159, 2014.
2. B.K. Alpert. A class of bases in  $L^2$  for the sparse representation of integral operators. *SIAM J. Math. Anal.*, 24(1):246–262, 1993.
3. N. Aronszajn. Theory of reproducing kernels. *Trans. Amer. Math. Soc.*, 68(3):337–404, 1950.
4. D. Baroli, H. Harbrecht, and Multerer. Samplet basis pursuit: Multiresolution scattered data approximation with sparsity constraints. *IEEE Trans. Sign. Proc.*, 72:1813–1823, 2024.
5. A. Berlinet and C. Thomas-Agnan. *Reproducing Kernel Hilbert Spaces in Probability and Statistics*. Springer Science & Business Media, New York, 2004.
6. G. Beylkin, R. Coifman, and V. Rokhlin. The fast wavelet transform and numerical algorithm. *Comm. Pure Appl. Math.*, 44:141–183, 1991.
7. P. Binev and R.A. DeVore. Fast computation in adaptive tree approximation. *Numer. Math.*, 97:193–217, 2004.
8. M. Blum, R.W. Floyd, V.R. Pratt, R.L. Rivest, and R.E. Tarjan. Time bounds for selection. *J. Comput. Syst. Sci.*, 7(4):448–461, 1973.
9. S. Börm. *Efficient Numerical Methods for Mon-Local Operators:  $\mathcal{H}^2$ -Matrix Compression, algorithms and analysis*. European Mathematical Society, Zürich, 2010.
10. D. Braess. *Finite Elemente. Theorie, schnelle Löser und Anwendungen in der Elastizitätstheorie*. Springer, Berlin-Heidelberg, 2013.
11. E. Candès, J. Romberg, and T. Tao. Stable signal recovery from incomplete and inaccurate measurements. *Comm. Pure Appl. Math.*, 59(8):1207–1223, 2006.
12. E.J. Candès and D.L. Donoho. Curvelets: A surprisingly effective nonadaptive representation for objects with edges. In A. Cohen, C. Rabut, and L. Schumaker, editors, *Curves and Surface Fitting: Saint-Malo 1999*, page 105–120, Nashville, 2000. Vanderbilt University Press.
13. J.C. Carr, R.K. Beatson, J.B. Cherrie, T.J. Mitchell, W.R. Fright, B.C. McCallum, and T.R. Evans. Reconstruction and representation of 3D objects with radial basis functions. In *Proceedings of the 28th annual conference on Computer graphics and interactive techniques, SIGGRAPH '01*, pages 67–76, New York, 2001. Association for Computing Machinery.
14. S. Chen and D.L. Donoho. Basis pursuit. In *Proceedings of 1994 28th Asilomar Conference on Signals, Systems and Computers*, volume 1, pages 41–44, Pacific Grove, CA, USA, 1994. IEEE.
15. S.S. Chen, D.L. Donoho, and M.A. Saunders. Atomic decomposition by basis pursuit. *SIAM J. Sci. Comput.*, 20(1):33–61, 1998.
16. C.K. Chui. *An Introduction to Wavelets*. Academic Press, San Diego, 1992.
17. C.K. Chui and E. Quak. Wavelets on a bounded interval. *Numer. Meth. Approx. Theory*, 9:53–75, 1992.
18. A. Cohen. *Numerical Analysis of Wavelet Methods*. Elsevier, Amsterdam, 2003.
19. R.R. Coifman and M. Maggioni. Diffusion wavelets. *Appl. Comput. Harmon. Anal.*, 21(1):53–94, 2006.
20. W. Dahmen. Wavelet and multiscale methods for operator equations. *Acta Numer.*, 6:55–228, 1997.
21. W. Dahmen, H. Harbrecht, and R. Schneider. Compression techniques for boundary integral equations. Optimal complexity estimates. *SIAM J. Numer. Anal.*, 43(6):2251–2271, 2006.
22. W. Dahmen, A. Kunoth, and K. Urban. Biorthogonal spline wavelets on the interval – stability and moment conditions. *Appl. Comp. Harm. Anal.*, 6(2):132–196, 1999.

23. W. Dahmen, S. Pröbldorf, and R. Schneider. Wavelet approximation methods for pseudodifferential equations II: Matrix compression and fast solution. *Adv. Comput. Math.*, 1(3):259–335, 1993.
24. W. Dahmen and R. Stevenson. Element-by-element construction of wavelets satisfying stability and moment conditions. *SIAM J. Numer. Anal.*, 37(1):319–352, 1999.
25. I. Daubechies. *Ten Lectures on Wavelets*. Society of Industrial and Applied Mathematics, Philadelphia, 1992.
26. I. Daubechies, M. Defrise, and C. De Mol. An iterative thresholding algorithm for linear inverse problems with a sparsity constraint. *Comm. Pure Appl. Math.*, 57:1413–1457, 2004.
27. R.A. DeVore. Nonlinear approximation. *Acta Numer.*, 7:51–150, 1998.
28. M.N. Do and M. Vetterli. The contourlet transform: An efficient directional multiresolution image representation. *IEEE Trans. Image Proc.*, 14:2091–2106, 2005.
29. D.L. Donoho. Compressed sensing. *IEEE Trans. Inf. Theory*, 52(4):1289–1306, 2006.
30. G.E. Fasshauer. *Meshfree Approximation Methods with MATLAB*. World Scientific, River Edge, 2007.
31. S. Foucart and H. Rauhut. *A Mathematical Introduction to Compressive Sensing*. Applied and Numerical Harmonic Analysis. Birkhäuser, New York, 2013.
32. A. George. Nested dissection of a regular finite element mesh. *SIAM J. Numer. Anal.*, 10(2):345–363, 1973.
33. K. Giebermann. Multilevel approximation of boundary integral operators. *Computing*, 67:183–207, 2001.
34. R. Griesse and D.A. Lorenz. A semismooth Newton method for Tikhonov functionals with sparsity constraints. *Inverse Problems*, 24(3):035007, 2008.
35. V. Guigue, A. Rakotomamonjy, and S. Canu. Kernel basis pursuit. In J. Gama, R. Camacho, P.B. Brazdil, A.M. Jorge, and L. Torgo, editors, *Machine Learning: ECML 2005*, pages 146–157, Berlin-Heidelberg, 2005. Springer.
36. K. Guo and D. Labate. Optimally sparse multidimensional representation using shearlets. *SIAM J. Math. Anal.*, 39(1):298–318, 2007.
37. W. Hackbusch and S. Börm.  $\mathcal{H}^2$ -matrix approximation of integral operators by interpolation. *Appl. Numer. Math.*, 43(1-2):129–143, 2002.
38. N. Hale, N.J. Higham, and L.N. Trefethen. Computing  $\mathbf{A}^\alpha$ ,  $\log(\mathbf{A})$ , and related matrix functions by contour integrals. *SIAM J. Numer. Anal.*, 46(5):2505–2523, 2008.
39. H. Harbrecht, U. Kähler, and R. Schneider. Wavelet Galerkin BEM on unstructured meshes. *Comput. Vis. Sci.*, 8(3-4):189–199, 2005.
40. H. Harbrecht and M. Multerer. A fast direct solver for nonlocal operators in wavelet coordinates. *J. Comput. Phys.*, 428:110056, 2021.
41. H. Harbrecht and M. Multerer. Samplets: Construction and scattered data compression. *J. Comput. Phys.*, 471:111616, 2022.
42. H. Harbrecht, M. Multerer, and J. Quizi. The dimension weighted fast multipole method for scattered data approximation. *arXiv:2402.09531*, 2024.
43. H. Harbrecht, M. Multerer, O. Schenk, and C. Schwab. Multiresolution kernel matrix algebra. *Numer. Math.*, 156(3):1085–1114, 2024.
44. H. Harbrecht and R. Schneider. Biorthogonal wavelet bases for the boundary element method. *Math. Nachr.*, 269(1):167–188, 2004.
45. H. Hersbach, B. Bell, P. Berrisford, S. Hirahara, A. Horányi, J. Muñoz-Sabater, J. Nicolas, C. Peubey, R. Radu, D. Schepers, A. Simmons, C. Soci, S. Abdalla, X. Abellan, G. Balsamo, P. Bechtold, G. Biavati, J. Bidlot, M. Bonavita, G. De Chiara, P. Dahlgren, D. Dee, M. Diamantakis, R. Dragani, J. Flemming, R. Forbes, M. Fuentes, A. Geer, L. Haimberger, S. Healy, R.J. Hogan, E. Hólm, M. Janisková, S. Keeley, P. Laloyaux, P. Lopez, C. Lupu, G. Radnoti, P. de Rosnay, I. Rozum, F. Vamborg, S. Villaume, and J.-N. Thépaut. The ERA5 global reanalysis. *Q. J. R. Meteorol.*, 146(730):1999–2049, 2020.
46. T. Hofmann, B. Schölkopf, and A.J. Smola. Kernel methods in machine learning. *Ann. Stat.*, 36(3):1171–1220, 2008.

47. L. Hörmander. *The Analysis of Linear Partial Differential Operators. I.* Classics in Mathematics. Springer, Berlin, 2003. Distribution theory and Fourier analysis, Reprint of the 1990 edition.
48. L. Hörmander. *The Analysis of Linear Partial Differential Operators. III.* Classics in Mathematics. Springer, Berlin, 2007. Pseudo-differential operators, Reprint of the 1994 edition.
49. G. James, D. Witten, T. Hastie, and R. Tibshirani. *An Introduction to Statistical Learning.* Springer Texts in Statistics. Springer, New York, 2013.
50. U. Kähler.  *$\mathcal{H}^2$ -Wavelet Galerkin BEM and Its Application to the Radiosity Equation.* Dissertation TU Chemnitz, Chemnitz, 2007.
51. G. Leobacher and F. Pillichshammer. *Introduction to Quasi-Monte Carlo Integration and Applications.* Springer International Publishing, Cham, 2010.
52. L. Lin, C. Yang, J. C. Meza, J. Lu, L. Ying, and W. E. Selin—*an algorithm for selected inversion of a sparse symmetric matrix.* *ACM Trans. Math. Softw.*, 37(4):40, 2011.
53. D.A. Lorenz. Convergence rates and source conditions for tikhonov regularization with sparsity constraints. *J. Inverse Ill-Posed Probl.*, 16(5):463–478, 2008.
54. S.G. Mallat. A theory for multiresolution signal decomposition: The wavelet representation. *IEEE Trans. Pattern Anal. Mach. Intell.*, 2(7), 1989.
55. S.G. Mallat. *A Wavelet Tour of Signal Processing.* Academic Press, San Diego, 1999.
56. S.G. Mallat. Understanding deep convolutional networks. *Philos. Trans. R. Soc. A*, 374(2065):2015.0203, 2016.
57. S.G. Mallat and Z. Zhang. Matching pursuits with time-frequency dictionaries. *IEEE Trans. Sign. Proc.*, 41(12):3397–3415, 1993.
58. C.A. Micchelli. Orthogonal projections are optimal algorithms. *J. Approx. Theory*, 40(2):101–110, 1984.
59. C.A. Micchelli and T.J. Rivlin. A survey of optimal recovery. In C.A. Micchelli and T.J. Rivlin, editors, *Optimal Estimation in Approximation Theory*, pages 1–54, New York, 1977. Springer.
60. K. Muandet, K. Fukumizu, B. Sriperumbudur, and B. Schölkopf. Kernel mean embedding of distributions: A review and beyond. *Found. Trends Mach. Learn.*, 10(1-2):1–141, 2017.
61. J.T. Schwartz N.J. Dunford. *Linear Operators. Part I: General Theory.* Interscience Publishers, New York, 1958.
62. I. Ram, M. Elad, and I. Cohen. Generalized tree-based wavelet transform. *IEEE Trans. Signal Process.*, 59(9):4199–4209, 2011.
63. R. Ramlau and G. Teschke. A Tikhonov-based projection iteration for nonlinear ill-posed problems with sparsity constraints. *Numer. Math.*, 104(2):177–203, 2006.
64. A.H. Robinson. A new map projection: Its development and characteristics. *International yearbook of cartography*, 14(1974):145–155, 1974.
65. L. Rodino. *Linear Partial Differential Operators in Gevrey Spaces.* World Scientific Publishing Co. Inc., River Edge, NJ, 1993.
66. R. Schaback and H. Wendland. Kernel techniques: from machine learning to meshless methods. *Acta Numer.*, 15:543–639, 2006.
67. R. Schneider. *Multiskalen- und Wavelet-Matrixkompression: Analysisbasierte Methoden zur Lösung großer vollbesetzter Gleichungssysteme.* B.G. Teubner, Stuttgart, 1998.
68. R.T. Seeley. Topics in pseudo-differential operators. In *Pseudo-Differential Operators (C.I.M.E., Stresa, 1968)*, page 167–305. Edizioni Cremonese, Rome, 1969.
69. C.E. Shannon. A mathematical theory of communication. *Bell Syst. Tech. J.*, 27(3):379–423, 1948.
70. T. Tao and E.J. Candès. Near-optimal signal recovery from random projections: universal encoding strategies? *IEEE Trans. Inf. Theory*, 52(12):5406–5425, 2006.
71. J. Tausch and J. White. Multiscale bases for the sparse representation of boundary integral operators on complex geometry. *SIAM J. Sci. Comput.*, 24(5):1610–1629, 2003.
72. M.E. Taylor. *Pseudodifferential Operators*, volume 34 of *Princeton Mathematical Series.* Princeton University Press, Princeton, NJ, 1981.
73. J.A. Tropp. Greed is good: algorithmic results for sparse approximation. *IEEE Trans. Inf. Theory*, 50(10):2231–2242, 2004.

74. T. von Petersdorff and C. Schwab. Fully discrete multiscale Galerkin BEM. In W. Dahmen, A. Kurdila, and P. Oswald, editors, *Multiscale wavelet methods for PDEs*, pages 287–346. Academic Press, San Diego, 1997.
75. T. von Petersdorff, C. Schwab, and R. Schneider. Multiwavelets for second-kind integral equations. *SIAM J. Numer. Anal.*, 34(6):2212–2227, 1997.
76. H. Wendland. *Scattered Data Approximation*. Cambridge University Press, Cambridge, 2004.
77. C.K. Williams and C.E. Rasmussen. *Gaussian Processes for Machine Learning*. MIT Press, Cambridge, 2006.
78. C.K.I. Williams. Prediction with Gaussian processes. From linear regression to linear prediction and beyond. In M.I. Jordan, editor, *Learning in Graphical Models*, volume 89 of *NATO ASI Series (Series D: Behavioural and Social Sciences)*. Springer, Dordrecht, 1998.